DRAFT   **IMECE2007-41038**

A NONEQUILIBRIUM THERMAL MODEL FOR RAPID HEATING AND PYROLYSIS OF ORGANIC COMPOSITES

Jianhua Zhou, Yuwen Zhang, J.K. Chen and D. E. Smith
Department of Mechanical and Aerospace Engineering
University of Missouri-Columbia
Columbia, MO 65211
zhangyu@missouri.edu

ABSTRACT

A nonequilibrium heat transfer model is developed to predict the through-thickness transient temperature variation in organic composites subjected to intensive heating. In addition to heat conduction, the model incorporates four important mechanisms: rate-dependent pyrolysis, pyrolysis byproduct outgassing, irradiance-dependent convection heat loss, and radiation heat lose. The heat conduction in the solid part is considered to be one-dimensional, and the compressible gas flow in the pyrolysis region is treated as two-dimensional. Both the shape of the gas flow channel and the gas addition velocity from the channel wall are evaluated based on the decomposition reaction rate. An iterative numerical procedure is formulated to solve the coupled heat transfer and gas flow equations. Numerical results, including the through-thickness temperature transients, the continually changing gas channel, and the pressure distribution in the decomposition gas are obtained and discussed.

INTRODUCTION

Advanced composites are a material in which two (or more) constituents are engineered to produce properties that would not be attained by conventional means [1]. For example, in carbon fiber-epoxy composites, carbon fibers are embedded in a matrix of epoxy to improve the rigidity and strength. To machine the composite materials into desired shapes, drilling and cutting are usually necessary to achieve the final surface quality and dimensional accuracy. Laser machining offers the advantages of high machining rates, no tool wear, no contact forces, and relatively high precision [2]. The effectiveness of laser machining depends primarily on the thermal and structural behaviors of the composite materials. Therefore, a comprehensive, accurate simulation tool is needed for evaluation and design of composites. Knowing the through-thickness transient temperature variation is a prerequisite for the subsequent laser ablation. Reed and Rice [3] developed a rate dependent pyrolysis model to characterize the heat transfer in decomposing material. Chen et al. [4] used a modified Crank-Nicholson finite difference scheme to model the heat transfer process in laser-irradiated composites. Although the heat transfer model [4] considered the effects of surface ablation, degradation of thermophysical properties at elevated temperatures, and radiation and convection heat losses, the cooling effect arising from the decomposition reaction outgassing was excluded. Recently, Zhou et al. [5] developed a two dimensional model to investigate the coupled compressible gas flow and heat transfer in a microchannel surrounded by solid media. The gas addition along the channel wall due to pyrolysis reaction was considered. However, the value of gas addition velocity and the cross-sectional area of the microchannel are assumed and not based on the pyrolysis reaction.

To overcome the drawbacks of the existing models, a numerical model based on the solution of the compressible Navier-Stokes equation is proposed. In addition to heat conduction, the model accounts four mechanisms: rate-dependent pyrolysis, pyrolysis byproduct outgassing, irradiance-dependent convection heat loss at the composite surface, and radiation heat loss at the composite surface. The heat conduction in the solid part is considered to be one-dimensional, and the pyrolysis gas flow is treated as a two-dimensional axisymmetric compressible flow in a microchannel with varying cross-section area, which is determined according to the decomposition reaction rate. The decomposition gas is added into the gas flow channel from the channel wall, and the gas addition velocity is estimated based on the decomposition reaction rate. The overall coupled heat transfer and gas flow problem is solved by using an iterative numerical algorithm.

NOMENCLATURE

A frequency factor in the rate equation

B activation energy parameter in the rate equation, K

c_p heat capacity at constant pressure, J/(kg·K)

h convection heat transfer coefficient, W/(m²·K)

h_{gas} convection heat transfer coefficient between the gaseous byproducts and the solid part of the composite, W/(m²·K)

$H(t)$ Heaviside step function

ΔH heat generated/absorbed by the decomposition reaction, J/kg

k thermal conductivity, W/(m²·K)

L thickness of the composite material, m

M the order of the pyrolysis reaction; or molar mass, kg/mol

p pressure, N/m²

Pr   Prandtl number

$q^{"}$ heat flux, W/m²

$\dot{Q}_{gas}$ heat source due to gas flow in the early stage of simulation, W/m³

$\dot{Q}_{pyro}$ heat source due to pyrolysis decomposition, W/m³

R_c radius of the gas flow channel, m

R_f outer radius of the unit cell, m

R_g gas constant, J/(kg·K)

t time, s

t_{pyro} pyrolysis onset time, s

T temperature, K

T_∞ ambient temperature, K

x, r coordinates in cylindrical coordinate system, m

u, υ velocity components in the axial and radial direction, respectively, m/s

$\mathbf{V}$ velocity vector, m/s

V_{add} gas addition velocity from channel wall, m/s

Greek symbols

γ heat capacity ratio

α fraction of the decomposed material

μ dynamic viscosity, kg/(m·s)

ε_{surf} surface emissivity

ρ mass density, kg/m³

σ Stefan-Boltzman constant, 5.67×10^{-8} W/(m²·K⁴)

∇ divergence operator

Subscripts

i initial

g gas

out outlet

s solid

$pyro$ pyrolysis decomposition

MODEL DESCRIPTION

The physical model is shown in Fig. 1 for a fiber composite material subjected to a localized heat flux q'', with a thickness of L and an initial temperature of T_i. Fig. 1(a) is a schematic of the composite before heating. The black regions represent fibers; the gray denotes the matrix. Fig. 1(b) shows the composite material after a heat flux is imposed on the top surface. Once the material is pyrolyzed, the pyrolyzed products are ejected as the gas flows outward from the pyrolysis zone toward the heated surface (the white regions in Fig. 1(b) represent the gas flow channels).

After the commencement of rapid heating, the entire material can be regarded as numerous inter-separated gas flow channels surrounded by the un-pyrolyzed solid materials, as shown in Fig. 1(b). Each gas flow channel, together with its surrounding material, constitutes an element (shown in the dash-line box of Fig. 1(b), as zoomed out in Fig. 1(c)). The diameter of each element is in micron scale and should be comparable to the fiber size.

Before the pyrolysis occurs, there is only pure conduction in the composite. When the temperature of the composite is elevated to the pyrolysis onset temperature, the composite material undergoes chemical decomposition. The decomposition process produces gaseous byproducts that flow outward from the pyrolysis zone toward the composite surface. Thus, there is a convection heat exchange between the solid part of the composite and the pyrolysis gas. The high-speed gas expelled at the surface will also increase the surface convection. Therefore, the surface convection heat loss must be considered as an irradiance-dependent process.

To describe the above-mentioned physical process, four mechanisms need to be considered in the heat transfer model: rate-dependent pyrolysis, pyrolysis byproduct outgassing, irradiance-dependent convection heat loss at the composite surface, and radiation heat loss at the composite surface.

Assume that a constant heat flux is specified at the top boundary (Fig. 1). The one-dimensional heat conduction in the solid part of the composite is governed by:

$$\rho_s c_{ps} \frac{\partial T_s}{\partial t} = \frac{\partial}{\partial x}(k_s \frac{\partial T_s}{\partial x}) + \dot{Q}_{pyro} H(t - t_{pyro}) + \frac{h_{gas}(T_g - T_s)}{R_f^2(1-\alpha)/2R_c} H(t - t_{pyro})$$

(1)

with an initial condition:

$$T_s = T_i \quad \text{for} \quad 0 \le x \le L, \quad t = 0 \tag{2}$$

and the boundary conditions:

$$-k_s \frac{\partial T_s}{\partial x} = q'' - h(T_s - T_\infty) - \varepsilon_{surf} \sigma(T_s^4 - T_\infty^4) \quad \text{for} \quad x = 0, \, t > 0 \tag{3}$$

$$-k_s \frac{\partial T_s}{\partial x} = h(T_s - T_\infty) + \varepsilon_{surf} \sigma(T_s^4 - T_\infty^4) \quad \text{for} \quad x = L, \, t > 0 \tag{4}$$
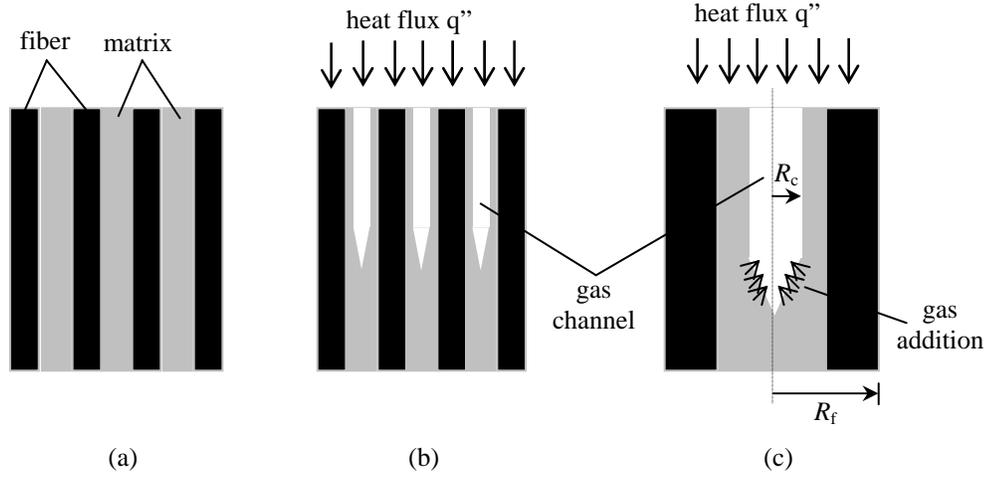
Figure 1 Physical model: (a) before heating, (b) after the commencement of heating, (c) zoom-out of a fiber-matrix element

Based on a 3-D porous material structure, the product of the density and the specific heat, i.e., $\rho_s c_{ps}$ in Eq. (1), is derived as:

$$\rho_s c_{ps} = (1-\alpha_{max})(\rho_s c_{ps})_f + \alpha_{max}(\rho_s c_{ps})_m$$
$$\text{in non-pyrolysis region} \quad (5)$$
$$\rho_s c_{ps} = (1-\alpha_{max})(\rho_s c_{ps})_f + (\alpha_{max}-\alpha)(\rho_s c_{ps})_m$$
$$\text{in pyrolysis region} \quad (6)$$

where α_{max} is the maximum fraction of the decomposed material. The subscripts f and m denote the fiber and matrix, respectively. The thermal conductivity k_s is temperature-dependent and will change as pyrolysis takes place. The thermal conductivity used in Ref. [4], with both temperature-dependence and effect of pyrolysis accounted for, is used in this work.

The pyrolysis is a rate-dependent process and the heat source term $\dot{Q}_{pyro}$ in Eq. (1) is calculated by:

$$\dot{Q}_{pyro} = -\frac{\rho_s \Delta H \cdot \dfrac{d\alpha}{dt}}{1-\alpha} = -\rho_s \Delta H \cdot A \cdot e^{\frac{B}{T} - M \cdot \int_{t_{pyro}}^{t} A e^{\frac{B}{T}} dt}/(1-\alpha) \quad (7)$$

The surface convection heat transfer coefficient, h, in Eq. (3) depends on the surface heat flux [6]. The convection heat exchange coefficient h_{gas} between the gas and the solid structure is evaluated according to the simulation results of the gas flow, i.e.:

$$h_{gas} = \frac{k_g}{T_s\big|_{r=R_c} - \overline{T}_g} \frac{\partial T_g}{\partial r}\bigg|_{r=R_c} \quad (8)$$

where k_g is the thermal conductivity of the gas; R_c is the radius of the gas flow channel, T_s and T_g are the temperatures of the solid and gas, respectively.

The radiation heat exchange at surface is proportional the fourth power of temperature. Instead of directly calculating the radiation loss with the nonlinear relation in Eqs. (3) and (4), the following equivalent convection coefficient is introduced:

$$q_{rad}^{''} = \varepsilon_{surf}\sigma(T_s^4 - T_\infty^4) = \varepsilon_{surf}\sigma(T_s^2 + T_\infty^2)(T_s + T_\infty)(T_s - T_\infty) = h_{equi}(T_s - T_\infty) \quad (9)$$

The above alternative ensures an unconditionally stable algorithm.

To obtain the gas temperature in Eq. (1) and its derivative in Eq. (8), we need to solve the fluid flow and heat transfer problem in the gas region. The 2D gas flow is assumed to be laminar and compressible. The continuity, momentum and energy equations for the compressible gas flow are expressed as follows [7]:

Continuity:

$$\frac{\partial \rho_g}{\partial t} + \frac{\partial}{\partial x}(\rho_g u) + \frac{\partial}{\partial r}(\rho_g \upsilon) = 0 \quad (10)$$

Momentum:

$$\frac{\partial}{\partial t}(\rho_g u) + \frac{\partial}{\partial x}(\rho_g uu) + \frac{1}{r}\frac{\partial}{\partial r}(\rho_g r\upsilon u) = -\frac{\partial p}{\partial x}$$
$$+ \mu\frac{\partial}{\partial x}(\frac{\partial u}{\partial x}) + \frac{\mu}{r}\frac{\partial}{\partial r}(r\frac{\partial u}{\partial r}) + \frac{\mu}{3}\frac{\partial}{\partial x}(\nabla \cdot \mathbf{V}) \quad (11a)$$

$$\frac{\partial}{\partial t}(\rho_g \upsilon) + \frac{\partial}{\partial x}(\rho_g u\upsilon) + \frac{1}{r}\frac{\partial}{\partial r}(\rho_g r\upsilon\upsilon) = -\frac{\partial p}{\partial r}$$
$$+ \mu\frac{\partial}{\partial x}(\frac{\partial \upsilon}{\partial x}) + \frac{\mu}{r}\frac{\partial}{\partial r}(r\frac{\partial \upsilon}{\partial r}) + \frac{\mu}{3}\frac{\partial}{\partial r}(\nabla \cdot \mathbf{V}) - \frac{\mu\upsilon}{r^2} \quad (11b)$$

Energy:

$$\frac{\partial}{\partial t}(\rho_g T_g) + \frac{\partial}{\partial x}(\rho_g u T_g) + \frac{1}{r}\frac{\partial}{\partial r}(\rho_g r \upsilon T_g) = -\frac{1}{c_{pg}}[\frac{\partial p}{\partial t} + \nabla \cdot (p\mathbf{V}) - p(\nabla \cdot \mathbf{V})]$$

$$+ \frac{k_g}{c_{pg}}\frac{\partial}{\partial x}(\frac{\partial T_g}{\partial x}) + \frac{k_g}{c_{pg}}\frac{1}{r}\frac{\partial}{\partial r}(r\frac{\partial T_g}{\partial r})$$

$$+ \frac{\mu}{c_{pg}}\left\{2\left[(\frac{\partial u}{\partial x})^2 + (\frac{\partial \upsilon}{\partial r})^2 + (\frac{\upsilon}{r})^2\right] + (\frac{\partial \upsilon}{\partial x} + \frac{\partial u}{\partial r})^2 - \frac{2}{3}(\nabla \cdot \mathbf{V})^2\right\}$$

$$(12)$$

The radius of the gas flow channel is not a constant and is determined by the fraction of the decomposition reaction:

$$R_c = \sqrt{\alpha} \cdot R_{fiber} \qquad (13)$$

in which α is the fraction of the decomposed material, which is evaluated based on the rate equation:

$$\frac{d\alpha}{dt} = A(1-\alpha)^M e^{B/T} \qquad (14)$$

where the constant B is determined by the activation energy and the universal gas constant.

The gas addition from the channel wall is determined by considering conservation of mass at the gas-solid interface, i.e.,

$$V_{add} = -\frac{1}{2}\frac{R_f^2}{R_c}\frac{\rho_s}{\rho_g}\frac{d\alpha}{dt} \qquad (15)$$

where the minus sign is a result of the fact that the gas is added in the negative radial coordinate. The decomposition fraction α is a function of time and space. This implies that the shape of the gas channel is time-varying and irregular. Therefore, it is required to describe the gas flow in a general curvilinear coordinate system. Equations (10)-(12) are thus transformed to the general curvilinear coordinate system by employing the chain rule. For brevity, the detailed transformation will not be given here.

As noticed, the gas mass addition due to the decomposition reaction is not implemented as a source term in the continuity equation. Instead, this effect is taken into account by introducing a non-zero velocity boundary condition at the gas channel wall.

If the channel is too narrow, the Knudsen number for the gas flow (defined as λ / L_c, where λ is the mean free path of the molecules and L_c is a characteristic length scale) will increase to a very large value. Under this circumstance, some microscopic flow effects (e.g., rarefaction) will become significant and the traditional Navier-Stokes equation will break down [8]. Therefore, in this study, in the early stage of the heating, the gas flow effect is approximated based on the energy conservation principle:

$$\dot{Q}_{gas} = \frac{\rho_{gas} R_c V_{add} c_{pg} dx(T_g - T_i)}{\frac{1}{2}R_f^2(1-\alpha)} \qquad (16)$$

When the gas channel size increases to a value that can be handled by the traditional Navier-Stokes equation, the gas flow field is solved by solving the Navier-Stokes equation.

The heat conduction in the solid region and the flow in the gas region are solved separately and then coupled at the solid-gas interface. No-slip flow boundary condition is imposed on the gas-solid interface. Because the Reynolds number is low for the microchannel gas flow, an underrelaxation technique is adopted to ensure a stable numerical algorithm. The time step is varied to capture the drastic temperature transients at the early stage of the rapid heating.

The governing Navier-Stokes equations are solved with the finite volume method (FVM) based on the SIMPLE algorithm [9]. The extension of the SIMPLE method by including the compressibility effect can be found in References [10-13]. The contravariant components of the velocity are used as the dependent variables in the momentum equations. The non-staggered grid arrangement is adopted where all variables are stored at the control volume geometrical center. The body-fitted mesh is generated using the multi-surface technique [14]. The momentum interpolation technique [15] is used to ensure a strong pressure-velocity coupling.

NUMERICAL ALGORITHM AND VALIDATION

As previously stated, the heat conduction in the solid region and the flow in the gas region are solved separately and then coupled at the solid-gas interface. Therefore, the overall solution process is an iterative one. The numerical solution procedure at each time step is as follows:

(1) Make an initial guess for the convection heat transfer coefficients at the solid-fluid interface.
(2) Perform the heat conduction simulation in the solid region.
(3) After step (2), the solid temperatures at the solid-gas interface are known. This serves as the temperature boundary condition for the gas region. Then, the compressible gas flow in the gas region is simulated. After doing this, the convection heat transfer coefficients at the solid-fluid interface are updated according to the temperature distribution in the gas region.
(4) Go back to step (2) and perform the heat conduction simulation in the solid region again with the most recently obtained convection coefficients, obtained from step (3), as the boundary condition,.

The foregoing solution process is repeated until the changes of the temperature in the solid region are smaller than a prescribed minor tolerance (e.g., 10^{-4}).

The FORTRAN computer codes are written based on the above-mentioned numerical method and procedure. In the following, the credibility of the computer codes for the 1D heat conduction and 2D axisymmetric compressible gas flow are verified against several test problems.

The first test problem is intended to test the effectiveness of the computer code in simulating the 1D heat conduction induced by high intensity laser heating with surface radiation

loss as in [4]. The calculating results show that good agreement is obtained between the present work and reference [4].

The second problem chosen is to measure the effectiveness of the computer code in predicting subsonic gas flows. This flow is considered for the 10% bump channel with implied exit Mach number 0.5, as in [13]. In this case, stagnation pressure and temperature are specified at the inlet. At the exit, all the variables are extrapolated except for the static pressure which is prescribed. Fig. 2 shows the comparison of the Mach number distributions between the algorithm results and those in [13]. It can be seen that these results agree very well.

(a)

(b)
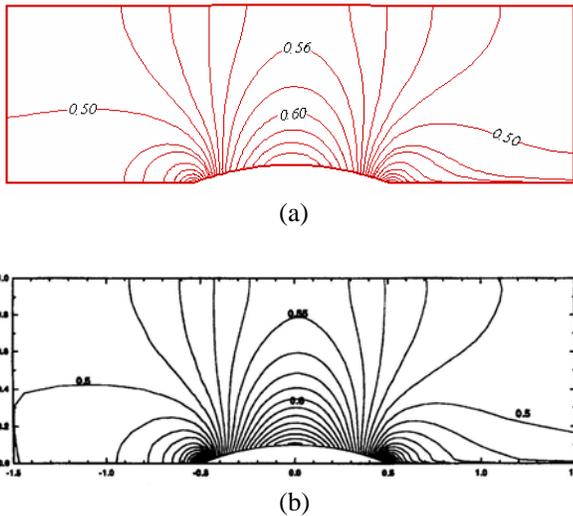
Figure 2 Mach number distributions for subsonic flow (10% bump channel). (a) Calculating results by present study and (b) Calculating results by Date [13]

The last test problem is for the supersonic flow in a 4% bump channel with an inlet Mach number 1.4 as in [13]. Since inlet Mach number is known, all variables at the inlet could be specified exactly. At the exit, all variables were linearly extrapolated. An 80×20 mesh is used for this case. The calculating results show that the shock wave effect due to supersonic flow is well captured using the present computer code. And once again, there is a good agreement between the present study and previous work [13].

RESULTS AND DISSCUSSIONS

Once the computer code is validated, the numerical analysis for a composite medium with 2.54 mm thickness is performed. The outer radius of the unit cell R_f is 400 μm. The material is initially at a uniform temperature, $T_i = 300K$. For time $t > 0$, a constant heat flux of $q'' = 5\ MW/m^2$ is impinged on the surface. After a grid convergence study, a 64×26 mesh is employed in the 2-D compressible gas flow and 41 grid points are used in the 1-D heat conduction simulation of the solid part. The numerical solution is started from time $t = 0$ with a varying time step Δt (a small time step is used in the initial stage since the temperature change during this stage is very drastic). The thermophysical properties of the solid composite used in the simulations are: $(\rho_s)_f = 1200$ kg/m³, $(c_{ps})_f = 1500$ J/(kg·K), $(\rho_s)_m = 800$ kg/m³, $(c_{ps})_m = 1100$ J/(kg·K). The physical properties of the gaseous byproducts are: $M = 28.97 \times 10^{-3}$ kg/mol, $c_{pg} = 1005$ J/(kg·K), $\text{Pr} = 0.7$, $\mu = 1.81 \times 10^{-6}$ kg/(m·s), $\gamma = 1.4$. Other data are as follows: The ambient temperature is $T_\infty = 300\ K$. The surface radiation emissivity is $\varepsilon_{surf} = 0.92$. The convection coefficient between the solid material and the ambient is $h = 5$ W/(m²·K) before onset of the pyrolysis reaction. The pyrolysis onset temperature is $T_{pyro} = 625K$. The decomposition reaction heat is: $\Delta H = 2 \times 10^6\ J/kg$. The order of the decomposition reaction is: $M = 1$. The maximum decomposition fraction α_{max} is 0.4. The frequency factor A in the rate equation is: $A = 1.243 \times 10^7$. The constant B in the rate equation is: $B = -1.17 \times 10^4$ K.
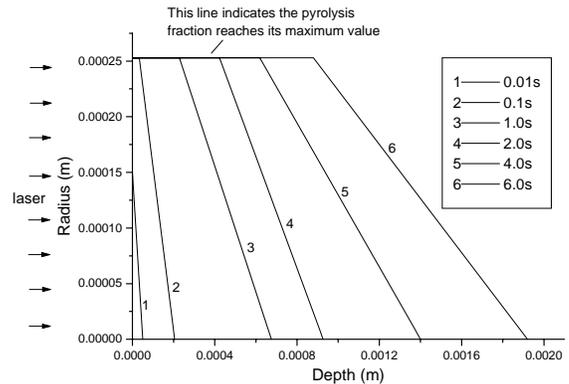

Figure 3 The progression of the pyrolysis front with time

Figure 3 shows the progression of the pyrolysis front as a function of time. It is clearly seen that the pyrolysis reaction front penetrates deeper and deeper into the composite as the heating proceeds. Such important information cannot be obtained by the one-dimensional gas flow approximation model. The horizontal line in Fig. 3 indicates that the fraction of the decomposed material reaches its maximum value. This leads to a straight gas channel section that has a constant cross-section area. It is worth noting that the pyrolysis front curve in Fig. 3 is fitted by a linear method. However, a much smoother pyrolysis front can be obtained by using a high order fit method at the expense of computer CPU time.

Figure 4 shows the predicted temperatures as a function of time at three different locations. It is clearly shown that the

temperature at the quarter depth is retarded over a range of temperatures during the endothermic decomposition reaction. The surface temperature increases drastically at the very beginning stage. This is because when the heating flux is very high, and thus there will be no sufficient time for the heat to be conducted into deeper depth. Eventually, all the temperatures reach a stable value. This indicates that the heat transfer process enters a quasi-steady state due to the combined effect of the heating, radiation loss, and gas flow cooling.
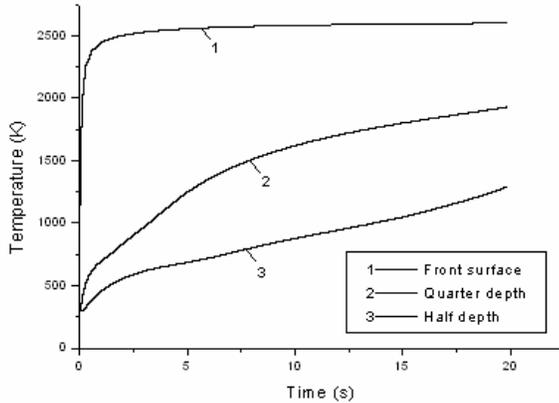
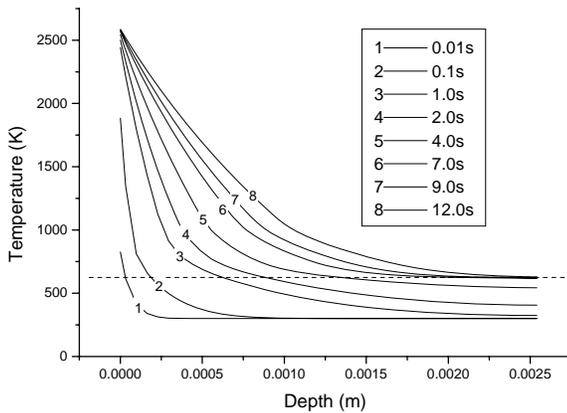**Figure 4** Predicted temperatures as a function of time at different locations

Figure 5 Spatial distribution of the temperature at different times

The spatial distributions of the temperatures at different times are plotted in Fig. 5. The decomposition reaction front is the intersection point between the temperature curve and the dashed line of the pyrolysis onset temperature. As time elapses, the decomposition reaction front penetrates deeper and deeper into the composite.

Figure 6 shows the gas addition velocity as a function of time at the depth of 0.16 mm. The minus sign of the gas

addition velocity is a result of the fact that the gas is added in the negative radius coordinate. It is seen that there is a small kink (at about 0.21 s) in the gas addition velocity profile. This can be explained as follows. The endothermic decomposition reaction results in a retarded temperature transient, as shown in Fig. 4. This retarded temperature variation, in turn, imposes a considerable influence on the rate equation, which induces an unsmooth fraction variation rate $d\alpha/dt$. Finally, such a fluctuant $d\alpha/dt$ leads to an unsmooth variation curve of gas addition velocity.
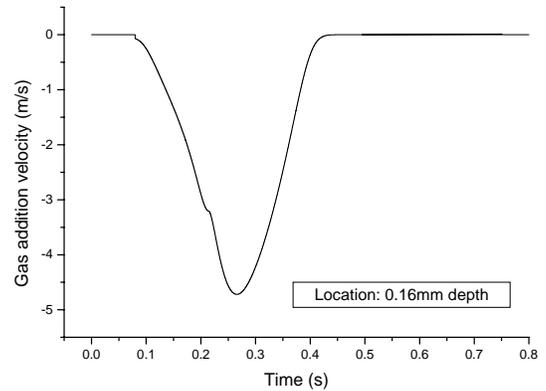

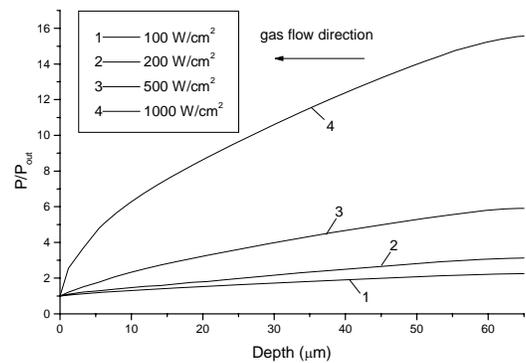**Figure 6** Gas addition velocity as a function of time

Figure 7 Centerline normalized pressure distribution for different heating flux

Figure 7 presents the centerline normalized pressure distribution for different heating fluxes at t = 10.6 s. It is seen from this figure that the pressure decreases gradually from the pyrolysis front to the heated surface. The higher the input heat flux, the larger the pressure difference from the pyrolysis front to the heated surface. This is because a higher heating flux causes a much more violent decomposition reaction, which, in turn, results in a higher gas addition velocity along the gas channel wall.

CONCLUSIONS

A nonequilibrium heat transfer model is developed to calculate the temperature transients in composites exposed to high heating flux. Besides the convection and radiation heat loss effects at surface, the pyrolysis gas flow effect is included into the model. The most striking feature of the present model is that both the shape of the gas flow channel and the gas addition velocity from the channel wall are evaluated based on the decomposition reaction rate. An iterative numerical procedure is formulated to solve the coupled heat transfer and gas flow problem. After the validation of the computer code, numerical simulations are performed for many cases. Important results, such as the through-thickness temperature transients, the time-varying gas channel shape, the pressure distribution in the decomposition gas, etc. are obtained and discussed. The pressure distribution along the channel axial direction is useful for further structural analysis of composite materials.

ACKNOWLEDGEMENT

REFERENCES

[1] Agarwal, B. D., and Broutman, L. J., 1990, *Analysis and Performance of Fiber Composites*, 2nd ed., John Wiley and Sons, New York.

[2] dell'Erba, M., Galantucci, L. M., and Miglietta, S., 1992, "An Experimental Study on Laser Drilling and Cutting of Composite Materials for the Aerospace Industry Using Excimer and CO_2 Sources," Composites Manufacturing, **3(1)**, pp.14-19.

[3] Reed, H. E., and Rice, M. H., 1993, "Failure of Solid Rocket Engines due to Laser Radiation Exposure," Cubed Report No. SSS-DFR-93-14222.

[4] Chen, J. K., Perea, A., and Allahdadi, F. A., 1995, "A Study of Laser/Composite Material Interactions," Composites Science and Technology, **54**, pp.35-44.

[5] Zhou, J., Zhang, Y., and Chen, J. K., 2007, "Numerical Simulation of Compressible Gas Flow and Heat Transfer in a Microchannel Surrounded by Solid Media," International Journal of Heat and Fluid Flow, in press.

[6] Smith, D. E., Zhang, Y., and Chen, J. K., *HELVAMP: Laser/Composite Interaction Research Project*, Final Technical Report Submitted to Air Force Research Laboratory/Ball Aerospace, July, 2006.

[7] Kays, W. M., and Crawford, M. E., 1980, *Convective Heat and Mass Transfer*, McGraw-Hill, New York.

[8] Harley, J. C., Huang, Y., Bau, H. H., and Zemel, J. N., 1995, "Gas Flow in Micro-Channels," Journal of Fluid Mechanics, **284**, pp.257-274.

[9] Patankar, S. V., 1980, *Numerical Heat Transfer and Fluid Flow*, Hemisphere, New York.

[10] Karki, K. C., and Patankar, S. V., 1989, "Pressure Based Calculation Procedure for Viscous Flows at All Speeds in Arbitrary Configurations," AIAA Journal, **27(9)**, pp.1167-1174.

[11] Demirdzic, I., Lilek, Z., and Peric, M., 1993, "A Collocated Finite Volume Method for Predicting Flows at All Speeds," International Journal for Numerical Methods in Fluids, **16**, pp.1029-1050.

[12] Rincon, J., and Elder, R., 1997, "A High-Resolution Pressure-Based Method for Compressible Flows," Computers and Fluids, **26(3)**, pp.217-231.

[13] Date, A. W., 1998, "Solution of Navier-Stokes Equations on Nonstaggered Grid at All Speeds," Numerical Heat Transfer, Part B, **33**, pp.451-467.

[14] Eiseman, P. R., 1985, "Grid Generation for Fluid Mechanics Computations," Annual Review of Fluid Mechanics, **17**, pp.487-522.

[15] Rhie, C. M., and Chow, W. L., 1983, "Numerical Study of the Turbulent Flow Past an Airfoil with Trailing Edge Separation," AIAA Journal, **21(11)**, pp.1525-1532.